Hindawi
Journal of Nanotechnology
Volume 2019, Article ID 2809867, 13 pages
https://doi.org/10.1155/2019/2809867

Review Article

Carbon Nanomaterials for the Adsorptive Desulfurization of Fuels

Efstratios Svinterikos,[1] Ioannis Zuburtikudis,[2] and Mohamed Al-Marzouqi[1]

[1]*Department of Chemical and Petroleum Engineering, United Arab Emirates University (UAEU), P.O. Box 15551, Al Ain, UAE*
[2]*Department of Chemical Engineering, Abu Dhabi University, Abu Dhabi, UAE*

Correspondence should be addressed to Ioannis Zuburtikudis; ioannis.zuburtikudis@adu.ac.ae

Received 8 October 2018; Accepted 10 January 2019; Published 3 February 2019

Guest Editor: Kunal Mondal

The increasing demand for cleaner fuels and the recent stringent regulations of commercial fuel specifications have driven the research of alternative methods to upgrade the current industrial desulfurization technology. Adsorptive desulfurization, the removal of refractory sulfur compounds using appropriate selective tailor-made adsorbents, has shown up as a promising alternative in the recent years. Carbon nanomaterials, namely, graphene, graphene oxide, carbon nanotubes and carbon nanofibers, show a significant potential as desulfurization adsorbents. Their surface area and porosity, their ability of easy functionalization, and their suitability to serve as a support of different types of adsorbents have rendered them attractive candidates for this purpose. In this review, after a presentation of the current industrial desulfurization practice and its limitations, the structure and properties of the carbon nanomaterials of interest will be described, followed by a detailed account of their applications in adsorptive desulfurization. The major literature findings and conclusions will be presented and discussed as a road map for future research in the field.

1. Introduction

1.1. The Problem of Sulfur in Fuels. Crude oil is a complex mixture consisting mainly of hydrocarbons, but it also includes a small yet significant amount of compounds which contain sulfur, oxygen, nitrogen, and metals. Generally, the range of sulfur content in crude oil is 0.05–10 wt.%, but most commonly it varies between 1 and 4 wt.% [1]. These crude oils that contain less than 1 wt.% sulfur are termed as sweet or low-sulfur, while those with more than 1 wt.% are termed as sour or high-sulfur. The sulfur compounds in petroleum can be either inorganic or organic. The former category includes elemental sulfur, COS (carbonyl sulfide), H_2S (hydrogen sulfide), and dissolved pyrites, while the latter includes compounds in which sulfur exists as a heteroatom bounded to a hydrocarbon molecule [1, 2]. Figure 1 summarizes the most common organic sulfur compounds encountered in crude oil. Alkyl-substituted derivatives of these molecules (not shown in Figure 1) are usually encountered, as well [3].

The presence of sulfur in crude oil poses a serious concern as it is associated with various problems and adverse effects. First, many sulfur compounds are harmful to human health. For example, heavier thiophenes are carcinogenic upon exposure of humans to certain levels [2]. Thiols have an unpleasant repulsive odor and they can cause nausea, breathing problems, irritation to the eyes, the throat, and the lungs, unconsciousness, and muscular spasms [2]. Moreover, sulfur compounds raise environmental concerns as they contribute to the atmospheric pollution. SO_2 is produced during combustion, which contributes to the phenomenon of acid rain and to the photochemical smog, two serious threats to the flora and fauna [2].

In addition, some compounds such as H_2S and lower aliphatic sulfides and mercaptans cause corrosion to the distribution pipelines and to the equipment of the refineries, increasing the maintenance costs and obstructing their operation [2]. A serious concern to many refining processes is also caused by the deleterious effect of sulfur compounds on catalysts. These molecules are selectively adsorbed on the

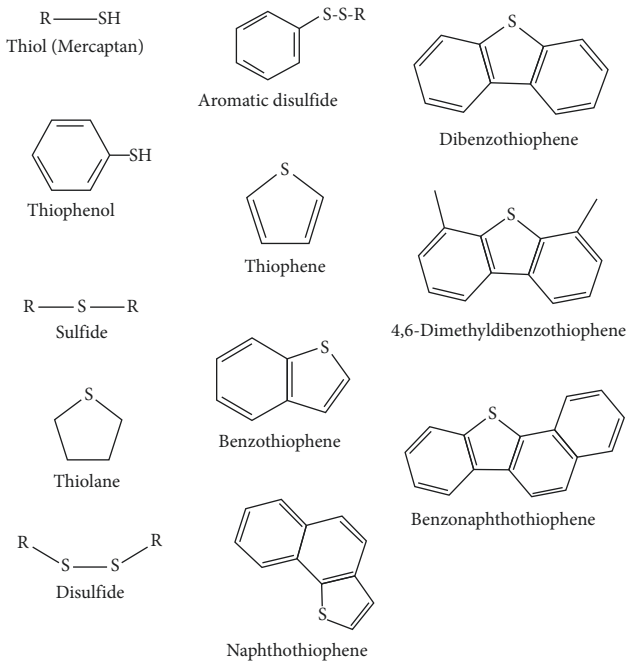

Figure 1: Common organic sulfur compounds in crude oil (taken from [1, 3]).

surface of metal catalysts, such as Cu, Ni, Co, Pb, Pt, and Ir, and they tend to deactivate them [2]. Finally, the presence of sulfur in gasoline tends to decrease its octane number; therefore, additional processing is required in order to reach the necessary specifications [2].

Because of the detrimental effects of sulfur compounds on human health and on the environment, the competent authorities in most countries apply regulations in order to limit the sulfur content of commercial fuels. These regulations become even more stringent with time, especially in the USA and in the EU. In the EU during the 90s, the maximum sulfur content for diesel was set to 350 ppm and for gasoline to 150 ppm [4]. Since 2009, however, the limit is 10 ppm for both fuels [5]. Similarly, in the USA, the current limits set by the US Environmental Protection Agency are set to 15 ppm for diesel and 10 ppm for gasoline [6, 7]. Moreover, the International Maritime Organization has decided to lower the limit of sulfur content for marine fuels from 3.5 wt.% to 0.5 wt.% starting in 2020 [8].

Furthermore, in the recent decades, there has been a growing interest in the development of fuel cells, aiming to the transition towards cleaner fuel technologies. Under this concept, research has focused on the development of cars based on hydrogen-powered fuel cells, such as polymer electrolyte membrane fuel cells (PEMFCs) and solid oxide fuel cells (SOFC) [3]. The problem is that these systems, which use hydrocarbon fuels as feedstock, are very sensitive to the presence of sulfur. PEMFCs demand a maximum sulfur content of 0.1 ppm, while solid oxide fuel cells can tolerate a maximum of 10 ppm [3]. Therefore, the regulations regarding the specifications of automobile fuels as well as the universal need to promote the use of cleaner fuels constantly drive the effort to develop more efficient technologies for deep desulfurization.

1.2. Desulfurization Strategies. Today, hydrodesulfurization (HDS) is the most common process in the refineries for the removal of sulfur compounds from petroleum distillates. This process was initially developed in the 1930s, and it is in use till now [3]. In HDS, the distillate is fed together with hydrogen gas in the catalytic reactor operating at elevated temperatures (320–440°C) and pressures (ranging from 15 up to around 200 atm) [2, 3]. The process conditions depend on the feedstock, with heavier petroleum fractions demanding higher operating temperatures and pressures [3]. Commonly used catalysts are sulfides of Mo or W supported on alumina and promoted by Co or Ni [3]. The HDS reaction proceeds through hydrogenation and hydrogenolysis [3].

Considering the variety of sulfur compounds found in petroleum and the differences in their structure and physicochemical properties, one should expect that each one exhibits different HDS reactivity. Indeed, HDS is very efficient for thiols, disulfides, and sulfides, because they have higher electron density of the S atom and weaker C-S bonds [3]. In contrast, in the thiophenic compounds, the S atom conjugates with the π-electrons of the aromatic ring; therefore, these bonds are stronger. There is also significant steric hindrance especially for the compounds which contain alkyl-substituents, so it is harder for the S atoms to reach the active centers of the catalyst. Hence, compounds such as 4,6-dimethyldibenzothiophene (higher thiophenes) present a very low HDS reactivity and are very difficult to be removed through this process; these compounds are termed as refractory sulfur compounds [3]. Table 1 shows the distribution of various sulfur compounds in different petroleum distillates, while Figure 2 summarizes the HDS reactivity of some representative molecules. Besides the problem of removing certain refractory compounds, reaching ultralow concentrations of sulfur is more difficult to be achieved with HDS, as it requires extreme operating conditions, that is, very high temperature and pressure, and higher consumption of catalyst and H_2, in order to remove a greater amount of sulfur [2, 3].

As a consequence, alternative ways for the efficient deep and ultradeep desulfurization of petroleum distillates have been investigated in the recent years. Some of the proposed alternatives are extractive desulfurization using specialized solvents, precipitative desulfurization, biodesulfurization using microorganisms, oxidative desulfurization, and adsorptive desulfurization on appropriate tailor-made adsorbents [2, 3]. Among these methods, the adsorptive desulfurization seems to be a very promising alternative to be used either alone or in conjunction with other methods, as it is less energy intensive, because it can be carried out under mild conditions of temperature and pressure, it does not require the consumption of H_2 or liquid solvents, and the adsorbents can be tailored for high selectivity of sulfur compounds [2, 3]. An example of adsorptive desulfurization used in the industrial scale is the S-Zorb process introduced by Phillips Petroleum Co. in 2001 in which selective adsorption is combined with hydrotreatment [2, 3]. Various researchers have focused on different adsorbents, including carbon nanomaterials, activated carbon, metal-organic frameworks, metal-oxide nanoparticles, and zeolites. For

Table 1: Distribution of sulfur compounds in different petroleum distillates (wt.%).*

Distillate fraction	Boiling point range (°C)	Thiols	Sulfides	Thiophenes	Higher thiophenes
Naphtha	70–180	50	50	Rare	—
Kerosene	160–240	25	25	35	15
Diesel	230–350	15	15	35	35
Vacuum gas oil	350–550	5	5	30	60
Vacuum residue	>550	Rare	Rare	10	90

*Taken from [2].

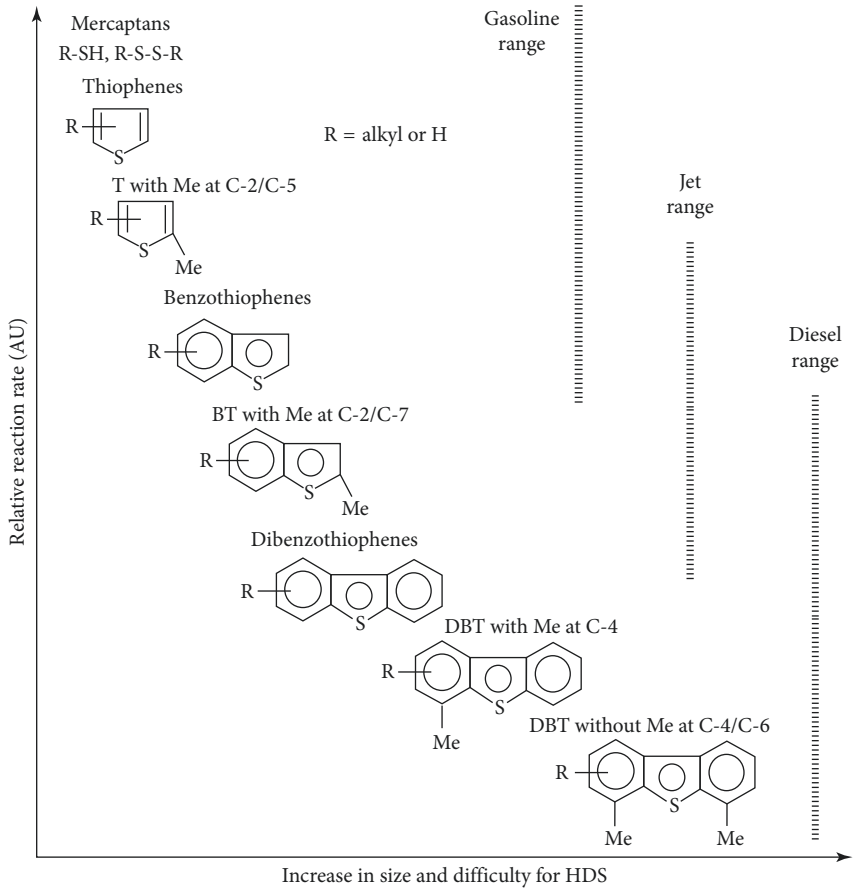

Figure 2: HDS reactivity of various organic sulfur compounds with respect to their ring sizes and alkyl substitutions. T: thiophene, BT: benzothiophene, DBT: dibenzothiophene, and Me: methyl-group (taken from [3]).

the purpose of this review, we will focus on carbon nanomaterials (graphene and graphene oxide, carbon nanotubes, and carbon nanofibers) that have been tested for the adsorption of sulfur compounds from petroleum distillates. The major findings reported in the literature will be summarized and discussed in the following sections, after a brief introduction to the structure and properties of the carbon nanomaterials of interest.

1.3. Carbon Nanomaterials

1.3.1. Graphene and Graphene Oxide. The discovery of graphene in 2004 was definitely followed by a scientific "hype" which continues until today, owing to its remarkable properties that are promising for a broad spectrum of technological applications. Graphene is a one-atom-thick 2D single layer of carbon atoms which are bonded into a hexagonal packed structure [9, 10]. The carbon bonds are sp^2-hybridized; this hybridization creates a structure with strong in-plane σ-bonds between the carbon atoms, and π-orbitals lying perpendicular to the plane [9, 10]. The π-orbitals are conjugated as in the aromatic molecules, and the π-electrons are delocalized on graphene surface. Hence, the σ-bonds combined build a rigid backbone of hexagonal structure, while the out-of-plane π-orbitals generate interactions between successive graphene sheets or with other molecules (e.g., aromatic rings) [9, 10]. Figure 3 depicts the graphene structure and bonding. Graphite consists of successive graphene sheets, stacked one on top of the other, bonded with weak van der Waals forces, in which the interlayer distance is around 0.34 nm [10].

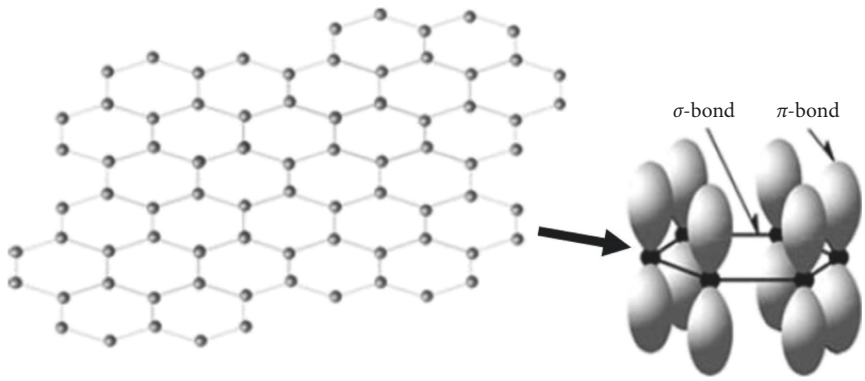

Figure 3: The graphene structure (taken from [10]).

Graphene has fueled intense research due to a combination of unique properties. To name a few of them [9–12], it is a zero-bandgap 2D semiconductor with a tiny overlap between valence and conduction bands; it is also highly transparent, and it exhibits a very high thermal conductivity (more than 3000 W/mK). It is completely impermeable to any gases, and it can sustain extremely high densities of electric current (1,000,000 times higher than copper). Its mechanical properties are unique, as its Young's modulus reaches the value of 1 TPa with an intrinsic strength of 130 GPa. The theoretical surface area of a single-layered graphene is very high (2630 m^2/g). It is hydrophobic, but it can be chemically functionalized. To its advantages, one should add the fact that the laboratory procedures for obtaining high-quality graphene are relatively cheap and simple [11]. However, most of these properties apply to the samples of highest quality and purity. This depends on the production method; the mechanical exfoliation of graphite gives graphene of the highest purity [11]. Other laboratory-scale production techniques include the liquid phase exfoliation of graphite, the chemical vapor deposition, and the synthesis on silicon carbide, but the industrial scale-up is an important issue [11]. A broader use of graphene in more specialized applications will be achieved, when it is feasible to produce graphene at an industrial scale with similar performance as the samples produced in research laboratories.

When graphite is oxidized through standard methods, such as the Hummer method, graphite oxide is produced [12]. Graphite oxide can then be exfoliated in organic solvents or water; therefore, single-layers of graphene oxide can be produced [12]. Graphene oxide is a functionalized form of graphene, which is decorated with oxygen-containing functional groups, most commonly hydroxyl and epoxy groups on the basal plane, and also carbonyl, carboxyl, phenol, lactone, and quinone groups at the edges [12]. Its exact atomic structure, however, cannot easily be identified. Figure 4 shows the structure of graphene oxide and its association with graphene.

This picture reveals that graphene oxide consists of a partially broken sp^2-carbon network. There is therefore a compromise on the remarkable physicochemical properties of graphene. However, the introduced surface functionalities render graphene oxide hydrophilic, in contrast to the hydrophobic graphene, so it can be well dispersed in polar solvents including water [12]. These functional groups can also initiate further functionalization or chemical modification.

1.3.2. Carbon Nanotubes. The 2D graphene is the building block for the graphitic materials of every other dimensionality. Hence, it can be wrapped into 0D fullerenes (buckyballs), rolled up into 1D nanotubes or stacked into the 3D graphite, building different architectures (Figure 5) [13].

As carbon nanotubes (CNTs) consist of rolled-up graphene sheets, they have the same sp^2-hybridized hexagonal structure, while their center is hollow. Generally, it has been found that when a graphene sheet consists of a relatively small number of carbon atoms, it is more thermodynamically stable if it closes onto itself forming a tubular architecture, in order to eliminate all hanging open bonds at the edges [14]. However, the rolling can occur at several manners, leading to various orientations of the lattice. Hence, with respect to the tube axis, the hexagonal arrays of carbon atoms follow a helical pattern on the tube surface. With respect to their helicity, CNTs can have a zigzag pattern, an armchair pattern, or a random helical one. The armchair CNTs have a metallic character with respect to their conductivity, while the others can be either metallic or semiconducting [14]. Moreover, regarding the number of graphene sheets building their structure, CNTs can be either single-walled (SWNT) or multiwalled (MWNT). SWNTs consist of a single graphene sheet rolled up, and they have a diameter of 1-2 nm. MWNTs consist of more than one parallel graphene sheets rolled up as concentric cylinders and their diameter is usually in the range of 2–25 nm [14]. The length of CNTs can reach several micrometers [14].

CNTs carry an array of fascinating properties comparable to graphene, such as very high in-plane thermal conductivity and Young's modulus [14]. Nevertheless, their electronic structure depends on their lattice helicity, and their density is smaller than that of graphite. The surface area of MWNTs has been measured to be around 10–20 m^2/g, while the surface area of SWNTs is around an order of magnitude larger [14]. These values are higher than those for

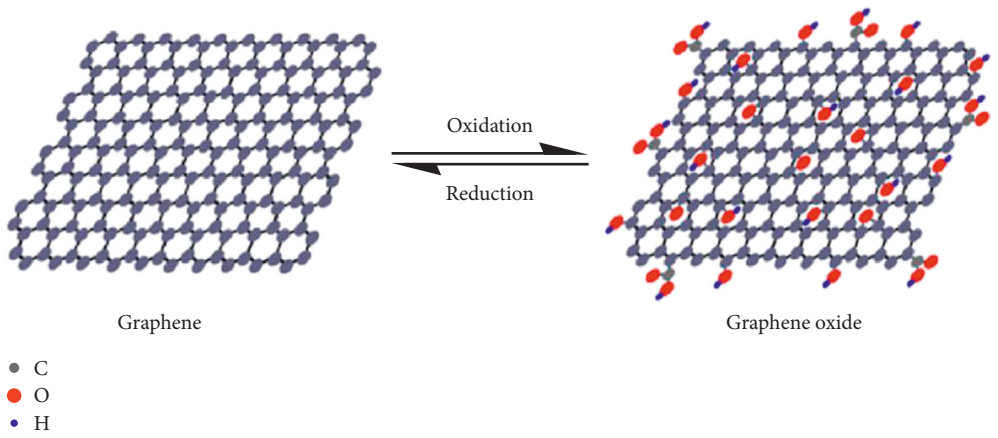

Figure 4: Structural model of graphene and graphene oxide (taken from [12]).

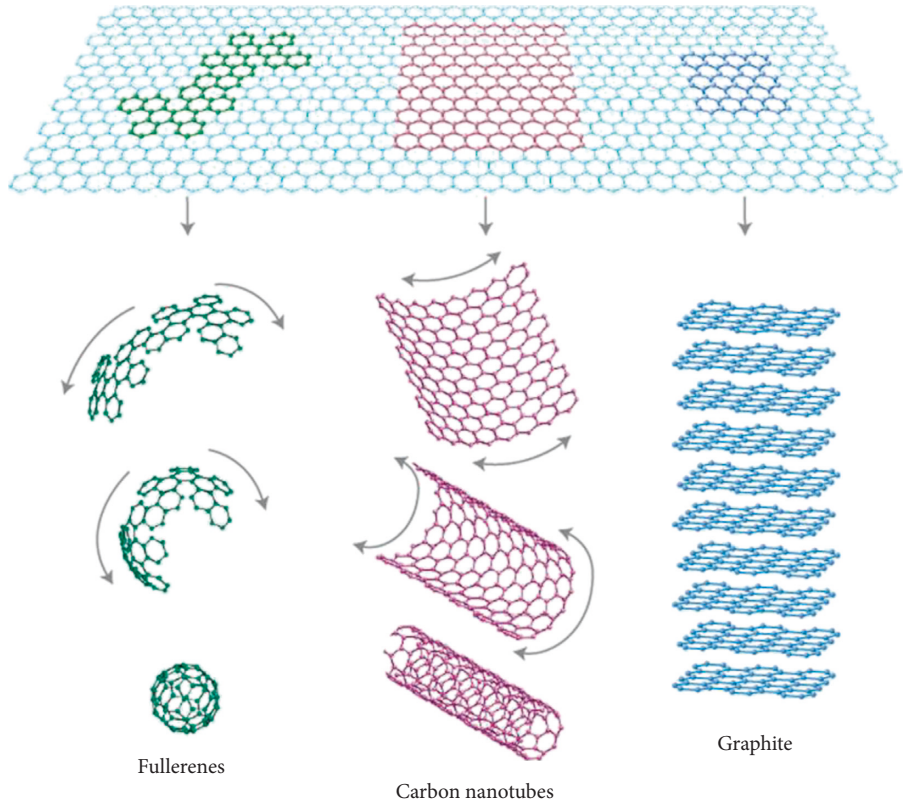

Figure 5: Graphene, the building block of all graphitic forms (taken from [13]).

graphite but smaller compared to those of activated porous carbon.

Furthermore, CNTs are insoluble to all organic solvents and aqueous solutions, but their surface can be modified or functionalized to alter their physicochemical properties [14, 15]. This modification usually belongs to one of the three following categories; (1) attachment of molecules through covalent bonds on the surface of the CNT, (2) noncovalent adsorption of functional molecules on the CNT, and (3) filling of their hollow cavity. In the case where the surface of CNTs is modified through covalent bonding with functional groups, a variety of reactions such as halogenation, hydrogenation, cycloadditions, addition of radicals or inorganic compounds, ozonolysis, grafting of polymers, esterification or amidation at their edges, and attachment of biomolecules have been reported [15]. Similarly, in the case of noncovalent bonding, it has been reported that the CNT surface can be covered by polymers, aromatic compounds, surfactants, or biomolecules through van der Waals forces or π-π stacking, in a way that their electronic network is not affected [15]. Finally, examples of filling their hollow cavity include the storage of liquid fuels or the encapsulation of fullerene derivatives, inorganic species, or biomolecules [15]. Therefore, CNTs are characterized by the susceptibility to

have their surface or cavity adjusted in various manners related to a specialized application.

1.3.3. Carbon Nanofibers. Carbon nanofibers (CNFs) are a high-added value form of carbon, which are applicable to various large-scale processes, including the manufacture of composites for the aerospace and automotive sectors and the adsorption of organic pollutants or heavy metals. They can also serve as substrates for catalyst support, and they can be used for energy storage, among others [16–18]. They have a diameter of few tens to few hundreds of nanometers, and their structure consists of graphitic and amorphous regions [16–18]. In this sense, their structure differs from that of carbon nanotubes, as in their case, their architecture and morphology are not entirely determined and defined to the atomic level. Instead, their structure is rather complex and varies from region to region inside each fiber. Inside the bulk of a CNF, crystallites consisting of bent layers of sp^2-hybridized carbon atoms exist (turbostratic regions); so, these regions resemble the form of graphite but contain many more defects [17]. Their structural characteristics, including the degree of crystallinity, the crystallite orientation and size, the extent of the amorphous regions, and the presence and geometry of pores, depend on their precursors, the method of manufacture, and possible posttreatment [16–19]. In Figure 6, a mat of carbon nanofibers is shown, together with a model of crystal structure for highly oriented carbon fibers.

CNFs carry a series of attractive properties, including high specific surface area, remarkable tensile strength and a modulus that can reach up to four times that of steel, low specific gravity, and high thermal stability [16, 19]. Moreover, their properties can be tailored according to the desired application by selecting the suitable precursors, adjusting the manufacturing method, or functionalizing their surface chemistry. The main manufacturing process of CNFs is the spinning and thermal treatment of a suitable polymeric precursor, such as poly(acrylonitrile), mesophase pitch, lignin, or their combinations with other polymers [17, 19]. The spinning of raw polymeric feedstock into polymeric precursor nanofibers is mainly carried out via electrospinning [16–19]. Electrospinning is advantageous in that the nanofiber diameter can easily be lowered to around 100 nm by adjusting the process parameters [20]. The precursor polymer nanofibers are then transformed to CNFs by heating them at high temperature (>600°C) under inert atmosphere [17, 19]. It has been reported that a graphitization step of thermal treatment at very high temperatures (~3000°C) leads to a more ordered graphitic structure, with a consequent improvement in their mechanical properties [17]. CNFs can also be synthesized via chemical vapor deposition (CVD). An activation step of heating under oxidizing atmosphere or of treatment with acids can significantly increase their surface area and introduce functional groups on their surface [17, 19].

The carbon nanomaterials described in the previous paragraphs have been tested for the removal of sulfur organic compounds from fuels, and they have exhibited promising potential. In the following sections, these results will be summarized and discussed.

2. Graphene Applications

As it was mentioned in the previous sections, graphene sheets consist of hexagonal carbon rings with π-orbitals lying perpendicular to their plane (Figure 3). This structure allows the bonding of molecules on graphene surface through π-π interactions (π-π stacking/π-π complexation). Graphene oxide, in contrast, due to the attachment of oxygen-containing functional groups allows π-π stacking to a much lesser extent than graphene, but the acidic or basic character of its functional groups is suitable for Lewis acid-base interactions with other molecules. Carboxyl-, lactone-, and phenol-groups have an acidic character, while ketone- and carbonyl-groups are basic [21].

Sulfur compounds such as H_2S and the various thiophenes and benzothiophenes have a basic character [22]. Therefore, their adsorption can be promoted, if the adsorbent has available acidic active sites (functional groups). Moreover, the refractory sulfur compounds, such as dibenzothiophene, contain aromatic rings which have conjugated π-orbitals available to develop π-π-interactions with the appropriate adsorbent [23]. In the majority of the scientific papers related to adsorptive desulfurization, the researchers focus on the adsorption of thiophene, dibenzothiophene of H_2S.

Song et al. studied the adsorption of dibenzothiophene (DBT) on graphene prepared from the reduction of graphene oxide [23]. Initially, graphite was oxidized using two different methods for the synthesis of graphene oxide, followed by reduction in order to produce graphene. The results showed that one of the methods led to graphene oxide with a higher degree of oxidation and increased interlayer spacing among the various layers. After reduction, this sample produced graphene with fewer defects, higher number of sp^2 carbons, and much higher specific surface area due to more efficient exfoliation (853.9 m^2/g vs. 394.9 m^2/g for the other sample). As a result, after the batch adsorption of DBT from a model fuel (n-tetradecane), it was found that the adsorption capacity of this graphene sample was almost twice compared to the more defective one (10.6 mgS/g vs. 5.5 mgS/g). The mechanism of the adsorption through π-complexation proposed by the authors is shown in Figure 7. This mechanism, however, has the disadvantage that in the case where the fuel contains aromatic compounds, as it happens with commercial fuels, there will be competitive adsorption; therefore, selectivity is an important issue. The researchers studied the adsorption of DBT from commercial diesel for comparison, and indeed the results showed that in that case the adsorption capacity of graphene fell to 3.3 mgS/g due to the presence of aromatics; therefore, the selectivity was low.

It has been reported that graphene oxide or graphite oxide, despite the presence of acidic functional groups, exhibits low adsorption capacity towards sulfur compounds [24–28]. This can be due to various reasons, such as the disruption of the hexagonal ring structure by the presence of functional groups, the inadequate degree of oxidation which leads to insufficient functional groups, and the inability to control the type of functional groups, or because of low

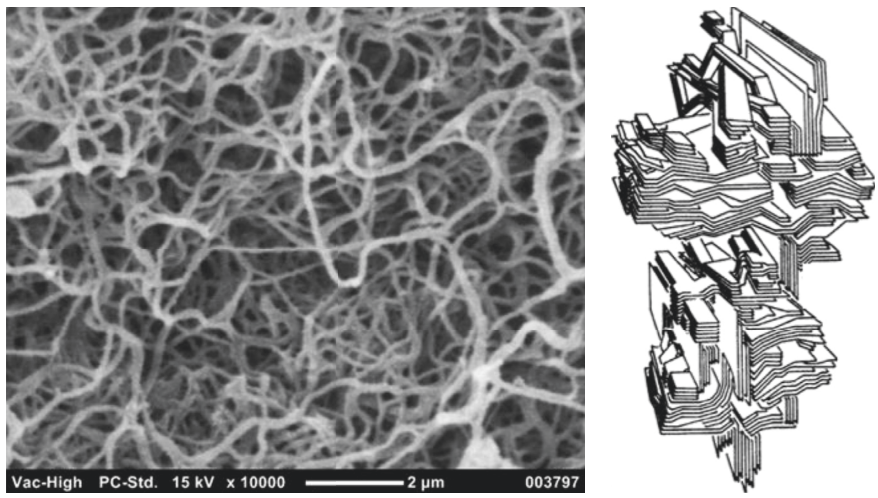

(a) (b)

Figure 6: (a) SEM image of a mat of carbon nanofibers with an average diameter of ~200 nm (image taken from our research group) and (b) model of the microscopic 3D carbon structure inside the bulk of a carbon fiber with graphitic and turbostratic layers (image taken from [17]).

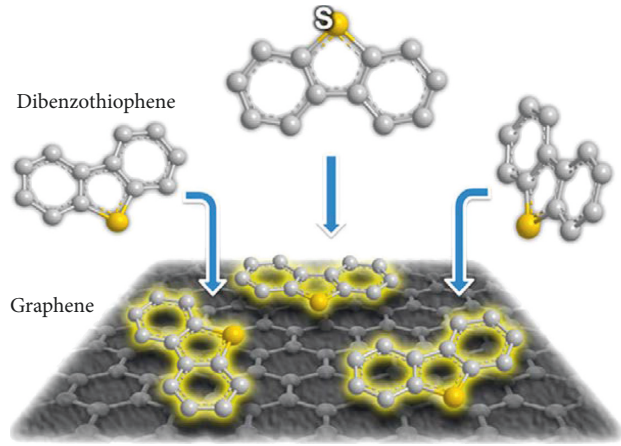

Figure 7: Adsorption of DBT on graphene via π-complexation (image taken from [23]).

specific surface area due to inadequate exfoliation of the layers [24–28]. However, different strategies can lead to the development of adsorbents with high adsorption capacity, by taking advantage of the intrinsic properties of graphene and graphene oxide. These strategies consist of using graphene or graphene oxide as a support for different adsorbents, such as metal oxides [24, 25, 27–29] or metal-organic frameworks (MOF) [26, 30, 31]; this synergy can boost their adsorption capacity.

Song et al. investigated the adsorption capacity of reduced graphene oxide/zinc oxide composites (rGO/ZnO) towards H_2S [24]. The process was carried out at an elevated temperature (300°C) because ZnO nanoparticles have been proven effective for hot-gas desulfurization of H_2S, which proceeds through the formation of zinc sulfide (ZnS). Adsorption tests with ZnO nanoparticles alone showed a reduced efficiency, probably because of particle aggregation. However, in the case of rGO/ZnO composite with 63.7 wt.% ZnO, the utilization efficiency of ZnO was 4 times higher. Therefore, rGO had a critical role in the efficient dispersion of the nanoparticles, and in the exposure of much higher active surface area for anchoring H_2S. The adsorption capacity in this case was 305 mgS/g-ZnO. Moreover, it was reported that the presence of H_2 assisted the adsorption, since its reducing effect provided more Zn^{2+} active sites, while the presence of CO_2 inhibited it through competitive adsorption.

In a similar way, Lonkar et al. report the successful adsorption of H_2S from a stream of methane gas on graphene/CuO composites [25]. Graphene was synthesized through thermal reduction of graphene oxide, the composite contained 10 wt.% of CuO, and the adsorption was carried out at room temperature. The results showed that the adsorption capacity of the composite was much higher than reduced graphene alone or pristine CuO alone. Graphene is crucial for the uniform dispersion of the oxide nanoparticles and the prevention of their aggregation, while the nanoparticles prevent the aggregation of graphene sheets, so, they can retain a high surface area. Some oxygenated functional groups existing on the surface of reduced graphene oxide possibly contribute to the initial physisorption of H_2S, which is then chemisorbed on CuO and converted to CuS (Figure 8). Here, the breakthrough capacity was measured 3 g-S/100 g-sorbent.

Ma et al. worked on a different approach regarding the rGO/CuO composite, in order to test it for the adsorption of DBT from model diesel (isooctane) [28]. DBT develops π-π interactions with the surface of rGO, which are desirable for its adsorption, but they render the regeneration of the adsorbent more difficult and energy intensive as these interactions are stronger than van der Waals forces. Therefore, they covered the surface of rGO with boehmite (γ-alumina) to prevent π-π stacking and added CuO as the active component for adsorption, because the bonds between CuO

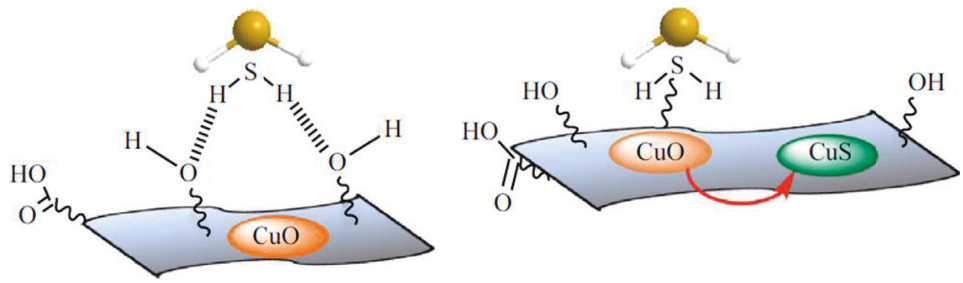

FIGURE 8: Mechanism of H_2S adsorption on reduced graphene/CuO composite through initial physisorption (a) and subsequent chemisorption (b) (image taken from [25]).

and DBT are moderate. The maximum adsorption capacity was measured at a 2 wt.% loading of CuO, and it was 6 mgS/g-adsorbent, 53% higher than the adsorption capacity of pure rGO (3.9 mgS/g-adsorbent). Regeneration of the adsorbent was performed through washing with toluene at 80°C, and it was shown that its capacity was reduced moderately after each cycle (~10%). In contrast, regeneration of pure rGO following the same process was unsuccessful, due to strong attachment of DBT molecules.

Menzel et al. used mixed metal oxides (MMO) supported on graphene oxide (MgAl-, CuAl-, and CoAl-MMO/GO) for the adsorption of DBT from dodecane [27]. The adsorption capacity of the hybrids was in all cases significantly higher compared to that of pristine-unsupported metal oxides and to that of pure GO. CuAl-MMO/GO exhibited the highest capacity normalized per unit of surface area, which was measured 0.333 μmol DBT/m^2 of adsorbent. The authors suggest that the boost in the adsorption performance caused by the presence of GO is not only due to the prevention of particle aggregation and the increase in their surface area alone, but it also appears to generate and stabilize some otherwise labile active sites. The same CuAl-MMO/GO composite exhibited high selectivity of DBT against aromatic hydrocarbons.

Nazal et al. prepared hybrids of GO with Al_2O_3, which has high thermal stability and can act as a Lewis acid (electron acceptor) due to its unsaturated surface [29]. The authors tested it for the adsorption of DBT from model fuel (n-hexane) and compared its performance to the adsorption capacities of carbon nanotubes loaded with Al_2O_3 and of activated carbon loaded with Al_2O_3. The best results were obtained for 5 wt.% loading of Al_2O_3 in all cases. The results revealed that the hybrid of GO/Al_2O_3 had the lowest adsorption capacity (29 mgDBT/g), while activated carbon/Al_2O_3 had the highest (85 mgDBT/g) and CNTs/Al_2O_3 had an intermediate one (41 mgDBT/g). These results were attributed to the large difference in the surface area; activated carbon/Al_2O_3 had 825 m^2/g, CNT/Al_2O_3 had 118 m^2/g, and GO/Al_2O_3 only 10 m^2/g. A high surface area is obviously crucial for every adsorption process. In the previous section, it was mentioned that graphene has a maximum theoretical surface area of 2630 m^2/g; this corresponds to totally exfoliated graphene sheets. However, when graphene layers are stacked one on top of one another, the surface area is compromised. Therefore, an efficient exfoliation of the layers is very important. In other studies, the GO hybrids have exhibited a much higher surface (for example 385 m^2/g [25] and 313 m^2/g [28]). Nazal et al. further report that in a real diesel sample, the adsorption capacity was generally reduced by around 30%, because of competitive adsorption with other aromatic or aliphatic sulfur compounds and probably due to an increased solubility of DBT in this medium which renders its diffusion to the adsorbent surface more difficult.

Besides the combination of graphene or graphene oxide with metal-oxide nanoparticles, another strategy has been reported for the development of efficient desulfurization adsorbents; the coupling of graphene or GO with metal-organic frameworks (MOFs). Huang et al. describe the synergy of GO with Zn-based MOF for the continuous removal of H_2S from N_2 [26]. MOFs are incapable of confining small molecules at ambient conditions due to weak dispersive forces. The presence of GO, at a 5.25 wt.% content, assisted in increasing these dispersive forces required for the retention of H_2S. Indeed, the breakthrough time of GO/MOF was much higher than that of MOFs alone or GO alone (171 min, 22 min, and 3 min respectively). The adsorption capacity was also significantly enhanced (130.1 mg/g, 16.7 mg/g, and 2.3 mg/g, respectively, for these three adsorbents). A GO mass ratio of just 5.25 wt.% in the hybrids gave the optimum capacity by contributing to a distortion of the MOF and to an increase in their surface area (1062 m^2/g compared to 812 m^2/g for pure MOF).

With a similar concept, Chen et al. combined GO with Cu-based MOF and tested them for the removal of thiophene from a model diesel fuel (n-octane) [30]. They report that adding 1.75 wt.% of GO in MOF, the adsorption capacity almost doubled (60.67 mg/g compared to around 35 mg/g for MOF alone). This effect is attributed to the significant increase in the surface are induced by the addition of GO (although further details are not provided by the authors).

Furthermore, Yang et al. synthesized a hybrid of hydroxylated graphene with Cu-based MOF and tested their adsorption performance for thiophene from model diesel fuel (isooctane) [31]. The addition of 6 wt.% of hydroxylated graphene increased the adsorption capacity of MOF to 35.6 mgS/g, while for MOF alone, it was measured 24.1 mg/g; the specific surface areas of these two hybrids were similar

(~968 m^2/g). The presence of graphene seems to modify the central metal and the unsaturated sites of the MOF. Probably, it also seems to protect the unsaturated sites from being occupied by unreacted organic ligands and solvent molecules, thereby increasing their exposure. Excess amount of graphene, however, seems to add some steric hindrance to MOF pores and blocks some of them. After being regenerated through washing with ethanol, the adsorbents showed good renewability as their adsorption capacity dropped by only 8% after five adsorption-regeneration cycles.

Besides the coupling of graphene or GO with metal oxides and MOF, their desulfurization capacity can be enhanced using different approaches such as the functionalization with ionic liquids or their doping with heteroatoms. Dizaji et al. functionalized GO in a noncovalent manner with imidazolium-based ionic liquids [21]. As it was mentioned in the previous section, noncovalent functionalization has a minimum impact in the structure and properties of GO and does not disrupt the π-conjugated bonds of its lattice. In this case, the noncovalent anchoring of the desired molecules proceeds either through van der Waals and cation-π interactions or through π-π stacking between the π network of imidazolium and the sp^2 network of GO. The hybrids of graphene oxide containing the highly electronegative bulky anion of [PF6] exhibited the highest adsorption capacity (6.5 mgS/g-adsorbent) of DBT from decane, and generally all samples of functionalized GO performed better than GO alone.

Applying a different idea, Shimoyama and Baba examined the ability of P- and N-doped graphite to adsorb thiophene vapor after previously placing the samples in an ultrahigh vacuum chamber [22]. The heteroatom doping was carried out through ion implantation using either phosphorus trichloride (PCl_3) vapor or N_2 gas. Experimental results and simulations revealed that thiophene adsorbs better at sites containing P, and in fact at curved P sites, as the thiophene adsorbed there tends to have a greater covalent bond character (higher adsorption energy). In contrast, thiophene molecules cannot be adsorbed at N sites. The results can be explained by the difference in the polarity of net charges between N and P sites. Regeneration of the adsorbent was successfully carried out by heat treatment at 800°C.

Hydrogenated graphene is termed as graphane, and it is synthesized when graphene is hydrogenated by exposure to hydrogen plasma [32]. Zhou et al. performed density functional theory (DFT) calculations for the adsorption of H_2S on graphane doped with transition-metal atoms (Fe, Co, and Cu) [32]. They found out that H_2S is strongly attached on these sites by chemisorption, therefore confirming the positive impact of transition metals on the adsorption of sulfur compounds on nanostructured carbon materials.

3. Carbon Nanotube Applications

In Section 1.3, it was described that carbon nanotubes consist of rolled-up graphene sheets; hence, their surface structure and their sp^2-hybridized hexagonal configuration are the same as graphene. Consequently, the utilization of CNTs in adsorptive desulfurization bears similarities to that of graphene, in that they are involved in π-π interactions, they can be functionalized, and they can be doped with nanoparticles to increase their adsorption capacity. However, as the specific surface area is important for adsorption, CNTs possess higher values of this property depending on the purification method. For purified SWNTs, values ranging from few hundreds of m^2/g up to around 1600 m^2/g have been reported [33].

Crespo et al. investigated the adsorption of various organic molecules, namely, benzene (aromatic), thiophene (heterocyclic), and cyclohexane (nonaromatic) on SWNTs of two different diameters (12 and 16.8 Å) [33]. The thinner nanotubes had a surface area of 961 m^2/g while the thicker ones had 322 m^2/g, which reflects the difference in the synthesis and purification methods. However, the authors normalized their adsorption results to per-area basis, in order to account for the difference in the surface area. Their results showed that narrower tubes adsorb larger amounts of adsorbates than the thicker ones, for all three organic compounds. This can be explained by the fact that in thinner SWNTs, the adsorbate molecules are exposed to a larger interaction potential from the delocalized electrons of the tubes. Moreover, the authors suggest that adsorption mainly occurs inside the nanotubes and to a smaller degree on their external surface or in the grooves among the nanotubes. Regarding the different adsorbates, there is no clear selectivity between the adsorption of benzene and thiophene. However, based on the measured heats of adsorption, thiophene was adsorbed more strongly on SWNTs. Both are adsorbed through π-interactions based on their aromaticity, while the nonaromatic cyclohexane is adsorbed to a smaller degree more weakly. The maximum theoretical adsorption capacity of thiophene on the thin SWNTs was 16.7 mmol/g estimated from Langmuir isotherms. The researchers also investigated the batch adsorption of thiophene from a model fuel (benzene) and also the desulfurization of a commercial diesel fuel (containing approximately 20% aromatics and 80% aliphatics, while the majority of sulfur compounds were various types of alkyl-dibenzothiophenes). In the model fuel, selectivity of thiophene over benzene was confirmed, which depends on the purification treatment of CNTs with HNO_3 that anchored some oxygen functional groups; the adsorption capacity was 0.86 mg thiophene/g. In the commercial diesel, the adsorption capacity was generally lower due to competitive adsorption. Comparing to activated carbon, it was found that heat-treated SWNTs performed better for the removal of heavier alkyl-DBTs.

Khaled [34] compared the adsorption capacity of commercial MWNTs with graphene oxide and activated carbon for the removal of thiophene and DBT from a model diesel fuel (*n*-hexane). In all three adsorbents, DBT was more favorably adsorbed than thiophene. According to the author, the reason is the difference in the dipole moment between the two molecules; thiophene has 0.55 D, while DBT has 0.95 D, so DBT develops stronger dipole-dipole interactions. The adsorption capacity of MWNTs for DBT was measured 23.42 mgDBT/g, close to the one of GO (22.73 mgDBT/g), but much lower than that of activated carbon (41.49 mgDBT/g).

It seems that activated carbon outperformed the other two adsorbents because of the large differences in their specific surface area (882 m^2/g for activated carbon, 217 m^2/g for MWNTs and 10.8 m^2/g for GO) and the average pore width (14.5 Å for activated carbon, 73.8 Å for MWNTs, and 68.5 Å for GO). It is important that the adsorbent should have a small average pore width comparable to the size of DBT molecules (<7 Å), so that the adsorbate will be trapped more efficiently. Here, activated carbon contained smaller pores on average, while its total micropore volume was much larger (0.487 ml/g compared to 0.286 ml/g for MWNTs and 0.021 ml/g for GO). Therefore, the differences in surface area, average pore width, and pore volume were crucial for the efficient removal of DBT in this case.

Nazal et al. also compared the adsorption efficiency between commercial CNTs and synthesized GO for the removal of DBT from heptane [35]. Their strategy, however, was different in that they doped these carbon nanomaterials with silver sulfide (Ag_2S) nanoparticles (10 wt.%). Ag, just like other transition metals such as Cu and Zn, can have a positive impact on adsorptive desulfurization. The results revealed that CNT/Ag_2S exhibited the highest adsorption capacity (52 mgDBT/g) slightly larger than GO/Ag_2S (49.6 mgDBT/g). However, compared to the capacities of raw CNTs and GO, which both were close to 23 mgDBT/g, it is obvious that the presence of Ag_2S almost doubled the removal efficiency of the adsorbents. The authors state that Ag^+ acts as a Lewis acid; its empty d-orbital is available to interact with the lone-pair sulfur electrons available in DBT (Lewis base). Probably, there was also a sulfur-sulfur interaction between the sulfur atom of DBT with the sulfur atom of Ag_2S.

Using a different approach, but of similar rationale as in the case of graphene, Meshkat et al. doped CNTs with N atoms and tested them for the removal of tertiary butyl mercaptan (TBM) from n-heptane [36]. The doping was carried out by adding urea during the CVD synthesis of CNTs. N atoms are incorporated into the CNT structure through pyridinic and pyrrolic N bonds, and their presence promotes the releasing of electrons; therefore, they can assist the adsorption of molecules through polar or acid-base interactions. The results revealed that the adsorption capacity of N-doped CNTs with 1.38 wt.% N-loading was 63.5 mgTBM/g, which was around 2.5 times higher than that of pure CNTs. As the electron density is increased locally on the surface of CNTs, these sites act as electron donors (Lewis base) and interact with the S atoms in TBM which are Lewis acids (electron acceptors). Moreover, it was measured that the doped N-CNTs had a specific surface area of 145.9 m^2/g, larger than that of undoped CNTs (74.4 m^2/g). Based on the adsorption kinetics, the authors suggested that the adsorption proceeds through two stages; a rapid diffusion on the external surface, followed by a slow pore diffusion.

4. Carbon Nanofiber Applications

A different kind of carbon nanomaterials used for the adsorptive desulfurization of fuels is that of carbon nanofibers (CNFs). Their most important characteristic is the relatively high specific surface area and porosity. Usually they are decorated with transition metals, such as Zn, Cu, or Ni, to enhance their adsorption capacity.

Kim et al. prepared carbon nanofibers decorated with ZnO nanoparticles for the adsorption of H_2S from a stream of nitrogen [37]. CNFs were prepared from the thermal treatment of poly(acrylonitrile) (PAN) nanofibers, which had been fabricated using the electrospinning technique. The decoration was carried out by adding zinc acetate dihydrate in the spinning solutions and a subsequent thermal treatment; the nanoparticle content on the surface of CNFs amounted to 13.6–34.2 wt.%. The average diameter of the various CNF samples was 152–304 nm, with the larger diameters appearing for the samples of higher ZnO content. Figure 9 shows TEM images of the CNFs containing different amounts of ZnO. It was found that when the ZnO content was increased, the average nanoparticle size also increased due to agglomeration; therefore, at 25.7 wt.% ZnO content, the nanoparticles had an average diameter of ~10 nm, while at a higher content, their average diameter increased to 50–80 nm, as more bulky clusters formed. Obviously, this is not desirable for the adsorption process, as a percentage of their surface is rendered inaccessible to the adsorbates and therefore useless.

As a result, the maximum breakthrough time, for a breakthrough concentration of 1 ppm, was observed for CNFs containing 25.7 wt.% ZnO (530 min/g-adsorbent), and it was significantly larger than the breakthrough time of undecorated CNFs (76 min/g-sorbent) or than that of pure ZnO (160 min/g-sorbent). In contrast, CNFs with a very high ZnO content of 34.2 wt.% showed a breakthrough time of only 143 min/g-adsorbent.

Bajaj et al. also utilized CNFs prepared from electrospun PAN, but their strategy was to decorate it with Cu/Cu_xO nanoparticles for the adsorption of H_2S [38]. The term "Cu/Cu_xO" denotes that after activation of the nanofibers, it was found that Cu nanoparticles were present together with their oxides on the nanofiber surface. Here, in contrast to the breakthrough time for pure CNFs, which was 62 min/g-adsorbent, the CNFs with 10 wt.% Cu/Cu_xO showed a breakthrough time of 791 min/g-adsorbent, while for those with 30 wt.% Cu/Cu_xO, it was 938 min/g-adsorbent, which is around 15 times higher than that of undecorated CNFs.

Karami et al. used commercial CNFs for the adsorption of 1-butyl mercaptan (1-butanethiol) from hexane, after first activating them through treatment with acids (HNO_3, H_2SO_4, and HCl) and decorating them with various amounts of Ni through electroless coating [39]. The adsorption studies showed that the CNFs which were coated with the highest amount of Ni (around 800 ppm) exhibited the highest percent of removal from the model diesel (~70%). Moreover, investigation of the adsorption kinetics revealed that increasing the amount of Ni in CNFs caused an increase in the adsorption rate constants, denoting the acceleration of the process. For first-order kinetics, CNFs containing ~300 ppm Ni had a rate constant of 0.7 s^{-1}, while for those with ~800 ppm, the rate constant was 2.3 s^{-1}.

Besides electrospinning, CNFs can be also synthesized via chemical vapor deposition (CVD). Bigdeli and Fatemi

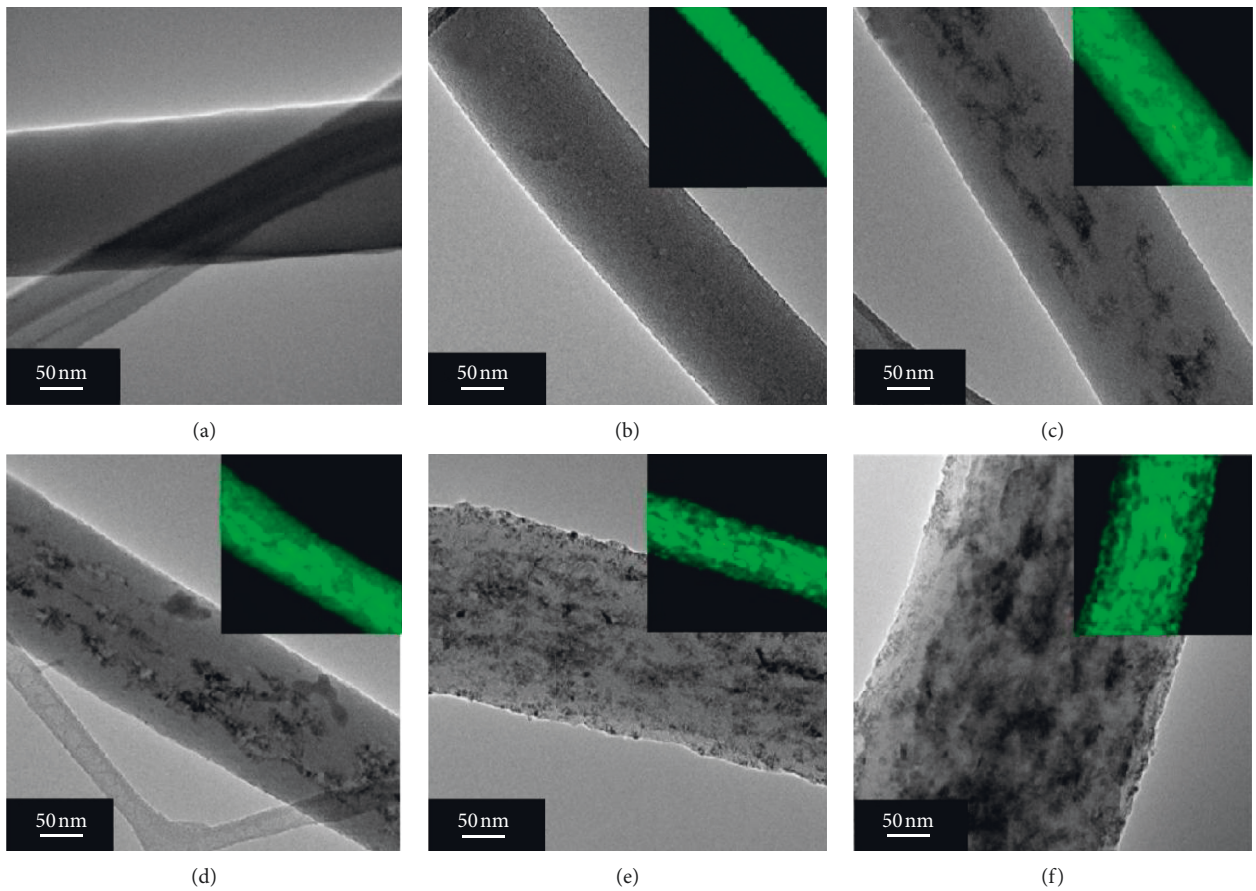

Figure 9: TEM images of CNFs containing ZnO nanoparticles of (a) 0, (b) 13.6, (c) 19.0, (d) 25.7, (e) 29.5, and (f) 34.2 wt.% (image taken from [37]).

used CVD to grow CNFs from methane and ethane gases on the surface of activated carbon, attempting to increase its surface area [40]. Here, Ni was used as a catalyst for CNF growth; therefore, activated carbon was first decorated with it. It was found that CNFs synthesized from methane gas were thinner (average diameters in the range of 45–55 nm) than those synthesized from ethane (120–190 nm). The presence of CNFs also significantly increased the specific surface area of the adsorbents, from the value of 529 m^2/g for the initial activated carbon, to 714 m^2/g for the sample containing CNFs synthesized from ethanol and 790 m^2/g for those synthesized from methane; the total pore volume was doubled, as well. These adsorbents were tested for the removal of thiophene or dibenzothiophene from n-octane. The results showed that the adsorption capacity of the CNF-containing samples was close to 13 mg/g for dibenzothiophene and close to 5 mg/g for thiophene; these numbers were almost double compared to the adsorption capacity of the initial activated carbon for both adsorbates. The higher adsorbed amount of DBT compared to thiophene can be attributed to its higher molecular weight, and to its plate shape, which allows more interactions with the adsorbent.

CVD-synthesized CNFs for the adsorption of thiophene from octane were also tested by Prajapati and Verma [41]. Here, Cu was used for the growth of CNFs, and then they were thermally treated for increasing their surface area and also decorated with Ni. Thermally treated Ni/Cu-CNFs exhibited a specific surface area of 346 m^2/g, much higher than the simple Cu-grown CNFs (107 m^2/g). This was obviously reflected to their adsorption capacity, which was 0.5 mgS/g with a breakthrough time of 130 min; in contrast, simple Cu-grown CNFs showed an adsorption capacity of 0.03 mgS/g and instant breakthrough. It was also found that increasing the temperature of adsorption from 30°C up to 200°C had an adverse effect on the process by decreasing the breakthrough time and adsorption capacity. It was therefore concluded that the adsorption of thiophene is exothermic and thus favorable at low temperatures.

The presence of CNFs is not always favorable for adsorption, as the process also depends on other characteristics such as the adsorbate characteristics or the substrate. Prajapati and Verma synthesized Ni-doped activated carbon beads with CNFs grown on them through CVD using acetylene [42]. CNFs were observed to be hollow, with average diameter close to 70 nm. While the starting activated carbon beads had a significantly large specific surface area (1159 m^2/g), when CNFs grew on them, their surface area dropped to around 500 m^2/g because many micropores were blocked. The authors used these adsorbents for the removal of thiophene from n-octane. The presence of Ni was proven

to boost the adsorption in all cases. The results showed that for DBT, the efficiency of the adsorbent containing CNFs was much smaller at all temperatures due to decreased surface area and total pore volume (8.2 mgS/g vs. 27.3 mgS/g for the case of activated carbon beads alone). In contrast, for the adsorption of thiophene, there was no significant difference in absolute numbers (capacity close to 86 mgS/g for each of them). Considering, however, that the adsorbent containing CNFs had much smaller surface area and pore volume, it seems that the capacity of CNFs was larger in this case. The most probable explanation is the difference in the molecular size between thiophene and DBT; thiophene is much smaller, so its adsorption is mostly dependent on the pore filling. Additionally, perhaps the interactions of thiophene with Ni were stronger in this case or possible interactions between thiophene and the graphitic planes of CNFs were helpful.

5. Concluding Remarks

As a conclusion, the desirable inherent properties of an adsorbent, that will enhance the efficiency of an adsorptive desulfurization process, include the following:

(a) Its high surface area

(b) Its high total pore volume

(c) Its high micropore volume

(d) The presence of oxygen-containing functional groups

(e) The presence of transition metals or metal oxides

(f) Possible doping with heteroatoms

(g) Its selectivity over aromatic or aliphatic hydrocarbons

(h) Its regenerability

(i) Its thermal stability when the process is conducted at high T

(j) Its low cost

Carbon nanomaterials possess most of these properties and the additional advantage that they can relatively easily be functionalized or modified to improve their performance. Their main disadvantage is probably the selectivity against aromatic components, while their regeneration is also an important factor to be considered. Nevertheless, they can provide an excellent substrate for the development of hybrids by combining them with other types of adsorbents, such as metal-organic frameworks or metal-oxide nanoparticles and boost their performance.

Generally, comparing the adsorption capacities of various adsorbents from literature values is not a reliable task, unless they are measured together for a specific system. The reason is that the adsorption capacity depends on various factors, such as the initial S concentration, the solvent or the type of fuel used, the type of sulfur compound, the presence of other competitive adsorbates such as aromatics, and so on. However, carbon nanomaterials seem to have the potential of industrial applications either alone or in combination with other adsorbents in a multistage process or even combining the adsorptive desulfurization with other processes such as oxidative desulfurization. Even so, established benchmark materials or long-standing processes can only be replaced when the new ones, although appealing, can be translated into processes that are competitive enough to justify the cost and disruption of replacing existing industrial practice.

Conflicts of Interest

The authors declare that there are no conflicts of interest regarding the publication of this article.

Acknowledgments

The authors would like to acknowledge the financial support provided by the Emirates Center for Energy and Environment Research (ECEER).

References

[1] M. Fahim, T. Al-Sahhaf, and A. Elkilani, *Fundamentals of Petroleum Refining*, Chapter 2, Elsevier, New York. NY, USA, 1st edition, 2010.

[2] W. Ahmad, "Sulfur in petroleum," in *Applying Nanotechnology to the Desulfurization Process in Petroleum Engineering*, S. Tawfik, Ed., IGI Global, Hershey, PA, USA, 2016.

[3] C. Song, U. Turaga, and X. Ma, "Desulfurization," in *Encyclopedia of Chemical Processing*, S. Lee, Ed., Taylor & Francis, Milton Park, UK, 2006.

[4] https://www.transportpolicy.net/standard/eu-fuels-diesel-and-gasoline/, accessed on 07/09/18.

[5] https://eur-lex.europa.eu/legal-content/EN/TXT/?uri=CELEX:32009L0030, accessed on 07/09/18.

[6] https://www.epa.gov/gasoline-standards/gasoline-sulfur, accessed on 07/09/18.

[7] https://www.epa.gov/diesel-fuel-standards/diesel-fuel-standards-and-rulemakings, accessed on 07/09/18.

[8] http://www.imo.org/en/MediaCentre/PressBriefings/Pages/MEPC-70-2020sulphur.aspx, accessed on 07/09/18.

[9] X. Huang, Z. Yin, S. Wu et al., "Graphene-based materials: synthesis, characterization, properties, and applications," *Small*, vol. 7, no. 14, pp. 1876–1902, 2011.

[10] W. Choi, I. Lahiri, R. Seelaboyina, and Y. S. Kang, "Synthesis of graphene and its applications: a review," *Critical Reviews in Solid State and Materials Sciences*, vol. 35, no. 1, pp. 52–71, 2010.

[11] K. S. Novoselov, V. I. Fal'Ko, L. Colombo, P. R. Gellert, M. G. Schwab, and K. Kim, "A roadmap for graphene," *Nature*, vol. 490, no. 7419, pp. 192–200, 2012.

[12] D. Chen, H. Feng, and J. Li, "Graphene oxide : preparation, functionalization, and electrochemical applications," *Chemical Reviews*, vol. 112, no. 11, pp. 6027–6053, 2012.

[13] A. Geim and K. Novoselov, "The rise of graphene," *Nature Materials*, vol. 6, pp. 183–191, 2007.

[14] P. M. Ajayan, "Nanotubes from carbon," *Chemical Reviews*, vol. 99, no. 7, pp. 1787–1800, 1999.

[15] D. Tasis, N. Tagmatarchis, A. Bianco, and M. Prato, "Chemistry of carbon nanotubes," *Chemical Reviews*, vol. 106, no. 3, pp. 1105–1136, 2006.

[16] B. Zhang, F. Kang, J. Tarascon, and J. Kim, "Recent advances in electrospun carbon nanofibers and their application in

electrochemical energy storage," *Progress in Materials Science*, vol. 76, pp. 319–380, 2016.

[17] E. Frank, L. M. Steudle, D. Ingildeev, J. M. Spörl, and M. R. Buchmeiser, "Carbon fibers: precursor systems, processing, structure, and properties," *Angewandte Chemie International Edition*, vol. 53, no. 21, pp. 5262–5298, 2014.

[18] M. Inagaki, Y. Yang, and F. Kang, "Carbon nanofibers prepared via electrospinning," *Advanced Materials*, vol. 24, no. 19, pp. 2547–2566, 2012.

[19] E. Svinterikos and I. Zuburtikudis, "Carbon nanofibers from renewable bioresources (lignin) and a recycled commodity polymer [poly(ethylene terephthalate)]," *Journal of Applied Polymer Science*, vol. 133, no. 37, pp. 1–12, 2016.

[20] E. Svinterikos and I. Zuburtikudis, "Tailor-made electrospun nanofibers of biowaste lignin/recycled poly(ethylene terephthalate)," *Journal of Polymers and the Environment*, vol. 25, no. 2, pp. 465–478, 2017.

[21] A. Khodadadi Dizaji, H. R. Mortaheb, and B. Mokhtarani, "Noncovalently functionalized graphene oxide/graphene with imidazolium-based ionic liquids for adsorptive removal of dibenzothiophene from model fuel," *Journal of Materials Science*, vol. 51, no. 22, pp. 10092–10103, 2016.

[22] I. Shimoyama and Y. Baba, "Thiophene adsorption on phosphorus- and nitrogen-doped graphites: control of desulfurization properties of carbon materials by heteroatom doping," *Carbon*, vol. 98, pp. 115–125, 2016.

[23] H. S. Song, C. H. Ko, W. Ahn et al., "Selective dibenzothiophene adsorption on graphene prepared using different methods," *Industrial & Engineering Chemistry Research*, vol. 51, no. 30, pp. 10259–10264, 2012.

[24] H. S. Song, M. G. Park, E. Croiset et al., "Effect of active zinc oxide dispersion on reduced graphite oxide for hydrogen sulfide adsorption at mid-temperature," *Applied Surface Science*, vol. 280, pp. 360–365, 2013.

[25] S. P. Lonkar, V. V. Pillai, S. Stephen, A. Abdala, and V. Mittal, "Facile in situ fabrication of nanostructured graphene–CuO hybrid with hydrogen sulfide removal capacity," *Nano-Micro Letters*, vol. 8, no. 4, pp. 312–319, 2016.

[26] Z. H. Huang, G. Liu, and F. Kang, "Glucose-promoted Zn-based metal-organic framework/graphene oxide composites for hydrogen sulfide removal," *ACS Applied Materials & Interfaces*, vol. 4, no. 9, pp. 4942–4947, 2012.

[27] R. Menzel, D. Iruretagoyena, Y. Wang et al., "Graphene oxide/mixed metal oxide hybrid materials for enhanced adsorption desulfurization of liquid hydrocarbon fuels," *Fuel*, vol. 181, pp. 531–536, 2016.

[28] H. Ma, X. Sun, M. Wang, and J. Zhang, "Regenerable CuO/γ-Al2O3-reduced graphene oxide adsorbent with a high adsorption capacity for dibenzothiophene from model diesel oil," *Industrial & Engineering Chemistry Research*, vol. 57, no. 32, pp. 10945–10955, 2018.

[29] M. K. Nazal, M. Khaled, M. A. Atieh, I. H. Aljundi, G. A. Oweimreen, and A. M. Abulkibash, "The nature and kinetics of the adsorption of dibenzothiophene in model diesel fuel on carbonaceous materials loaded with aluminum oxide particles," *Arabian Journal of Chemistry*, 2015, In press.

[30] M. Chen, Y. Ding, Y. Liu, N. Wang, B. Yang, and L. Ma, "Adsorptive desulfurization of thiophene from the model fuels onto graphite oxide/metal-organic framework composites," *Petroleum Science and Technology*, vol. 36, no. 2, pp. 141–147, 2018.

[31] K. Yang, Y. Yan, W. Chen et al., "Nut-like MOF/hydroxylated graphene hybrid materials for adsorptive desulfurization of thiophene," *RSC Advances*, vol. 8, no. 42, pp. 23671–23678, 2018.

[32] Q. Zhou, X. Su, W. Ju et al., "Adsorption of H_2S on graphane decorated with Fe, Co and Cu: a DFT study," *RSC Advances*, vol. 7, no. 50, pp. 31457–31465, 2017.

[33] D. Crespo and R. T. Yang, "Adsorption of organic vapors on single-walled carbon nanotubes," *Industrial & Engineering Chemistry Research*, vol. 45, no. 16, pp. 5524–5530, 2006.

[34] M. Khaled, "Adsorption performance of multiwall carbon nanotubes and graphene oxide for removal of thiophene and dibenzothiophene from model diesel fuel," *Research on Chemical Intermediates*, vol. 41, no. 12, pp. 9817–9833, 2015.

[35] M. K. Nazal, M. Khaled, I. H. Aljundi, M. Atieh, G. A. Oweimreen, and A. M. Abulkibash, "Synthesis of silver sulfide modified carbon materials for adsorptive removal of dibenzothiophene in n-hexane," *Environmental Technology*, vol. 38, no. 23, pp. 2949–2963, 2017.

[36] S. S. Meshkat, A. Rashidi, and O. Tavakoli, "Removal of mercaptan from natural gas condensate using N-doped carbon nanotube adsorbents: kinetic and DFT study," *Journal of Natural Gas Science and Engineering*, vol. 55, pp. 288–297, 2018.

[37] S. Kim, B. Bajaj, C. K. Byun et al., "Preparation of flexible zinc oxide/carbon nanofiber webs for mid-temperature desulfurization," *Applied Surface Science*, vol. 320, pp. 218–224, 2014.

[38] B. Bajaj, H. I. Joh, S. M. Jo, J. H. Park, K. B. Yi, and S. Lee, "Enhanced reactive H_2S adsorption using carbon nanofibers supported with Cu/Cu_xO nanoparticles," *Applied Surface Science*, vol. 429, pp. 253–257, 2018.

[39] F. Karami, M. Khanmohammadi, and A. B. Garmarudi, "ATR-FTIR spectroscopy and chemometrics application for analytical and kinetics characterization of adsorption of 1-butyl mercaptan (1-butanethiol) on nickel coated carbon nanofibers (CNFS)," *Bulgarian Chemical Communications*, vol. 48, pp. 51–56, 2016.

[40] S. Bigdeli and S. Fatemi, "Fast carbon nanofiber growth on the surface of activated carbon by microwave irradiation: a modified nano-adsorbent for deep desulfurization of liquid fuels," *Chemical Engineering Journal*, vol. 269, pp. 306–315, 2015.

[41] Y. N. Prajapati and N. Verma, "Fixed bed adsorptive desulfurization of thiophene over Cu/Ni-dispersed carbon nanofiber," *Fuel*, vol. 216, pp. 381–389, 2018.

[42] Y. N. Prajapati and N. Verma, "Adsorptive desulfurization of diesel oil using nickel nanoparticle-doped activated carbon beads with/without carbon nanofibers: effects of adsorbate size and adsorbent texture," *Fuel*, vol. 189, pp. 186–194, 2017.